Segmentation of vessel-like patterns using mathematical morphology and curvature evaluation

2 authors, including:

Jean-Claude Klein
MINES ParisTech
64 PUBLICATIONS   **2,716** CITATIONS

Segmentation of Vessel-Like Patterns Using Mathematical Morphology and Curvature Evaluation

Frédéric Zana and Jean-Claude Klein

Abstract—This paper presents an algorithm based on mathematical morphology and curvature evaluation for the detection of vessel-like patterns in a noisy environment. Such patterns are very common in medical images. Vessel detection is interesting for the computation of parameters related to blood flow. Its tree-like geometry makes it a usable feature for registration between images that can be of a different nature. In order to define vessel-like patterns, segmentation will be performed with respect to a precise model. We define a vessel as a bright pattern, piece-wise connected, and locally linear. Mathematical Morphology is very well adapted to this description, however other patterns fit such a morphological description. In order to differentiate vessels from analogous background patterns, a cross-curvature evaluation is performed. They are separated out as they have a specific Gaussian-like profile whose curvature varies smoothly along the vessel. The detection algorithm that derives directly from this modeling is based on four steps:

   1) noise reduction;
   2) linear pattern with Gaussian-like profile improvement;
   3) cross-curvature evaluation;
   4) linear filtering.

We present its theoretical background and illustrate it on real images of various natures, then evaluate its robustness and its accuracy with respect to noise.

Index Terms—Blood, edge detection, image analysis, mathematical morphology, ophthalmology, vessels.

I. INTRODUCTION

A. Edge Detection

EDGE detection is an essential task in computer vision. It covers a wide range of applications, from segmentation to pattern matching. It reduces the complexity of the image allowing more costly algorithms like object recognition [1], [2], object matching [3], object registration [4], or surface reconstruction from stereo images [5], [6] to be used. Vessel-like patterns with a Gaussian-like profile are very common, especially in medical images. Their detection is interesting for different goals. They can be used to measure parameters related to blood flow or to locate some patterns in relation to the vessels in angiographic images. They can also be used as a first step before registration [4], [7], [8]. A robust algorithm, suitable for different types of images, should allow registration of retinal images of very different nature and should permit one to combine information from data provided by various sources. In the case of eye

fundus images, the detection of the vascular tree seems a natural approach to the registration problem. Vessels are the only features that are common to every image of the retina. This is particularly true for angiographic images, since the signal comes from a dye injection.

In this paper, we present an algorithm that combines Morphological filters and cross-curvature evaluation to segment vessel-like patterns. Its application to images from retinal angiographies has been briefly presented in [9]. We study the behavior of this algorithm on a wider set of angiographic images and we extend its range to other images of the retina. Vessel-like patterns are bright features defined by morphological properties: linearity, connectivity, width and by a specific Gaussian-like profile whose curvature varies smoothly along the crest line. We use mathematical morphology to highlight vessels with respect to their morphological properties. We then evaluate the cross curvature. Vessels are detected as the only features whose curvature is linearly coherent. This algorithm has been tested on retinal photographs of three different types: fluoroangiography, gray images obtained with a green filter, and color images with no filter. Occasionally a short preprocessing step was necessary since the algorithm only works with bright patterns in gray level images. We then evaluate the behavior of this algorithm with respect to different kinds of noise, in order to measure its robustness and its accuracy. Finally, we compare this algorithm to other methods and we present a conclusion.

B. Morphological Operators

This section is a short reminder of some basic definitions of extensive morphological operators. More details can be found in [10].

We define a two-dimensional (2-D) image whose range is $[N_{\min}, N_{\max}]$ as a functional $S: \mathbb{R}^2 \to [N_{\min}, N_{\max}]$, and a 2-D structuring element as a functional $B: \mathbb{R}^2 \to \boldsymbol{B}$ where $\boldsymbol{B}$ is the set of the neighborhoods of the origin. In our approach we will only consider structuring elements invariant by translation, that are thus identified with a subset of $\mathbb{R}^2$, and we will refer to linear structuring elements when this subset is a segment.

We then define basic operators, with respect to the structuring element B with scaling factor e, image S and point $M_0 \in \mathbb{R}^2$:

erosion: $\epsilon_B^e(S)(M_0) = \text{MIN}_{M \in M_0 + e \cdot B(M_0)}(S(M))$;

dilation: $\delta_B^e(S)(M_0) = \text{MAX}_{M \in M_0 + e \cdot B(M_0)}(S(M))$;

opening: $\gamma_B^e(S) = \delta_B^e(\epsilon_B^e(S))$;

closing: $\phi_B^e(S) = \epsilon_B^e(\delta_B^e(S))$;

top-hat: $TH_B^e(S) = S - \gamma_B^e(S)$.

We will not use superscripts for unit scaling factor. Geodesic operators are defined with respect to a norm $||\cdot||$, or a connectivity

graph in digitized images (a neighborhood C of unit radius). They depend on a marker image S_m and distance d.

The geodesic dilation $S^d = \Delta^d_{S_m}(S)$ is defined by

$$S^1(M_0) = \inf(\{\text{MAX}_{M \in M_0 + C}(S_m(M))\}, S(M_0))$$
$$S^{d+1}(M_0) = \Delta^{d+1}_{S_m}(S)(M_0) = \Delta^1_{S_m}(S^d)(M_0).$$

The geodesic reconstruction (or opening) is defined by

$$\gamma^{rec}_{S_m}(S) = \sup_{d \in \mathbb{N}}(\Delta^d_{S_m}(S)).$$

The geodesic closing is defined by

$$\phi^{rec}_{S_m}(S) = N_{\max} - \gamma^{rec}_{(N_{\max} - S_m)}(N_{\max} - S).$$

II. VESSEL-LIKE PATTERN DESCRIPTION

A. Crest Lines and Rotating Matched Filters

Much has been written about detection of edges with a Gaussian-like profile. At least three different methods were applied to vessel segmentation: crest line detection [7], rotating matched filters [11], and neural networks [12]. Both methods [7] and [11] use linear operators and are based on differential properties. The crest line approach is based on the detection of the Gaussian profile by the use of up to the third derivative. Crest lines are lines where the magnitude of the maximum curvature is locally maximum in the corresponding principal direction (definition of [7]). This yields edges that are not necessarily connected. Rotating matched filters have been applied to the green plane of color eye fundus images in order to detect patterns with Gaussian profile across a constant line. Those matched filters are based on results and theory described in [8] and [2]. In this case, vessels can be very well highlighted, however further treatments, specific to the data, are necessary to remove other undesired linear features. We will show that the use of some morphological filters leads to an image simplification that eases the computation of cross-curvatures. Based on this observation, we have developed an algorithm based on a precise description of vessel-like patterns and look-alike background elements that combines morphological and differential properties.

B. Vessel-Like Pattern Modeling

We assume that the vascular tree is the only element of our image that is locally uniform in color or gray value completely described by the following properties (see Fig. 1):

- the shape of a cross-section looks like a Gaussian curve;
- it is connected in a tree-like way;
- vessels have a certain width and cannot be too close together.

These properties can be separated into those related to the morphological description (linearity, connectivity, vessel width) and those related to the calculation of some parameters (the curve of the Gaussian profile, its variation along the crest lines).
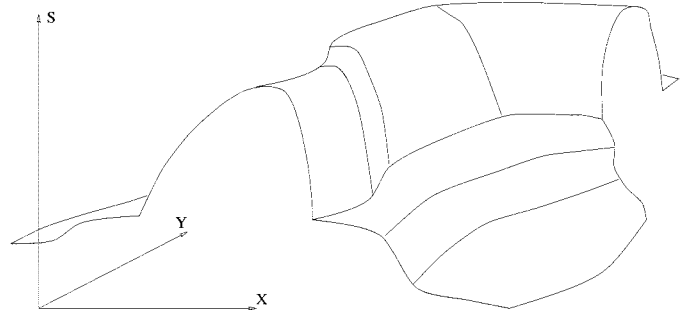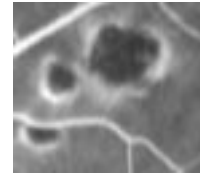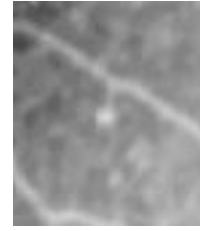

Fig. 1. Model of vessel.

(a)

(b)

(c)

Fig. 2. Various background textures. (a) Image with an addition of dark regions surrounded by a bright gray value. (b) Regular background noise, with some capillaries. (c) Smooth texture with linear features in the background.

There are different kinds of undesirable patterns encountered when extracting the vascular tree. We have classified them into different cases m that we will refer to in this article.

Case 1) Noise occurring during the digitization process, or due to undesirable elements whose texture can be described by a low intensity white noise.

Case 2) Background linear features that can be confused with vessels in some parts, but that do not meet all the requirements (they can be too thin or too close).

Case 3) Other kinds of patterns that are not linear. We can separate them into three subcases:

   case a) large bright or dark areas;
   case b) bright or dark thin irregular zones;
   case c) small bright or dark areas.

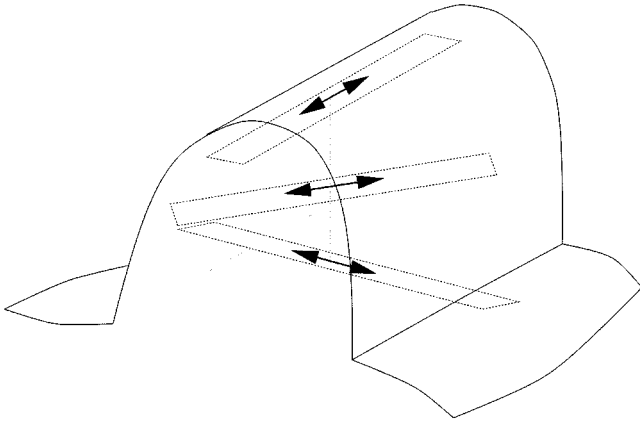Case 4) Low signal/noise ratio concerning the intensity of vessels (see Figs. 2 and 9).

Fig. 3.   Openings using linear structuring elements.

III. TREATMENT OF RETINAL FLUORESCEIN ANGIOGRAPHIES

A. Images of Retinal Fluorescein Angiographies

Images of retinal angiographies are obtained after an injection of fluorescein into the left arm. Retinal vessels are highlighted using an ultraviolet light. The diffusion process lasts a few minutes: after 5 min, the signal is very weak and noisy. Another difficulty is due to the histology of the eye, which is composed of several layers. The layers below the retina create background noise whose characteristics may vary significantly among people.

Therefore, a sequence of photographs taken during a 5-min injection gives adequate material for vessel detection under a noisy environment with various signal intensities. The size of the detected vascular structure, in angiographic images, is related to the degree of diffusion of the dye into the vessels. It can also be used as a preprocessing step of a registration algorithm (see [13]). Later on, we will use this algorithm on other retinal images.

B. Morphological Treatment for the Recognition of Geometric Features

Because of the linear property of vessels, we use morphological filters with linear structuring elements.

1) Recognition of Linear Parts: Linear bright shapes can easily be identified using mathematical morphology. An opening using a linear structuring element will remove a vessel or part of it when the structuring element cannot be included inside the vessel, as is the case when they have orthogonal directions and the structuring element is longer than the vessel width. Conversely, when the structuring element and the vessel have parallel directions, the vessel will stay nearly unchanged (see Fig. 3). If we consider the openings along a class of linear structuring elements, a sum of top-hats along each direction will brighten the vessels regardless of their direction. However, this operation requires the length of the structuring elements to be large enough to remove big vessels, hence we will recover a lot of noise in the sum of top hats. In order to deal with this problem, we preprocess the image using the connectivity property (Fig. 4).
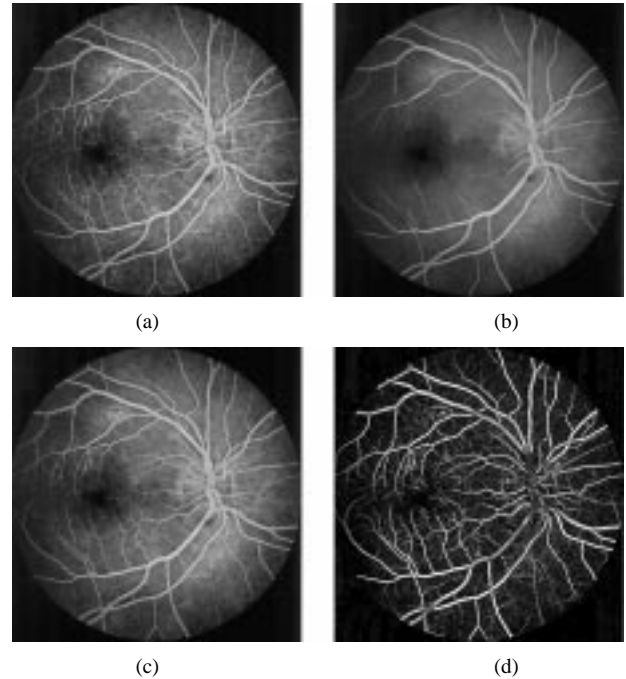

(a)

(b)

(c)

(d)

Fig. 4.   Each step of the morphological treatment: (a) initial image, (b) supremum of opening, (c) reconstruction, and (d) sum of top-hats.

2) Using the Connectivity Property: We remove noise while preserving most of the capillaries using a geodesic reconstruction of the opened images into the original image S_0:

$$S_{op} = \gamma_{S_0}^{rec}(\text{Max}_{i=1\ldots12}\{\gamma_{L_i}(S_0)\}).$$

Each structuring element L_i (every 15°) is 15-pixels long (1-pixel wide). Its size is approximately the range of the diameter of the biggest vessels for $512 \times 512 \times 8$ images of retinal angiographies, as explained in [11]. In the image S_{op}, every isolated round and bright zone whose diameter is less than 15 pixels has been removed. Being a supremum of openings by reconstruction this operation is an opening (see [10]), called *linear opening by reconstruction* of size 15. Removed elements include white noise (case 1) and some abnormalities (case 3c).

The sum of tophats on the filtered image S_{op} will enhance all vessels whatever their direction, including small or tortuous vessels, even in the low signal (case 4). The large homogeneous pathological areas (case 3b) will be set to zero since they are unchanged by γ_{L_i}, however the S_{op} image contains a lot of details corresponding to case 2 and possibly case 3b that are also enhanced by the difference.

3) Using Differential Properties as a Separating Tool: We assume at this stage that any nonzero point in the picture has a dominant direction, and thus can be considered as part of some lengthened pattern (vessels, patterns 2 or 3b). We will refer to the *curvature* whenever it is the curvature in the cross direction, which is now defined for every pixel under the former assumption. Its evaluation using the Laplacian will be discussed in the following section. In case 3b [Fig. 5(b)], the signal appears as thin and irregular bright linear elements, therefore the curvature gets positive values on a width smaller than in the case of the vessels (see Fig. 6), and it is not necessarily linearly correlated.
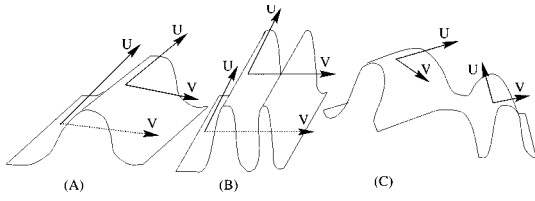
Fig. 5. (a) Vessel and (b) and (c) cases 3b and 2 from Section II-B. U and V are the principal directions.
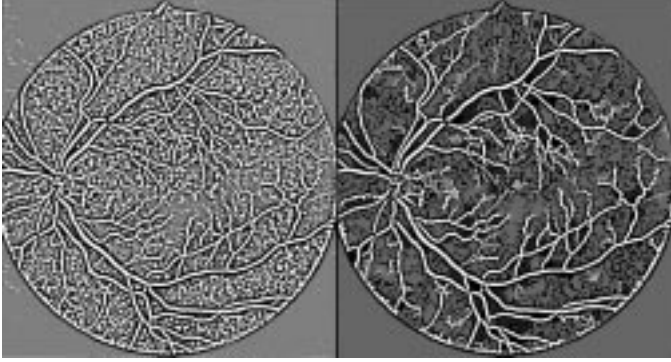

Fig. 6. Laplacian images highlighted around zero (positive values in white and negative values in black) before and after the alterning filter.

In case 2 [Fig. 5(c)], the signal tends to be low and disorganized, and the curvature will have alternating positive and negative values in various directions: linear morphological openings performed on the curvature image are very well adapted to such treatments. However, in a few cases, this fuzzy signal can have a curvature that looks very much like a small vessel. Our strategy does not separate this signal from the retinal vessels [Fig. 5(a)],leading to false detection that is hopefully rare and isolated.

After computing a Laplacian, we obtain a good estimation of the curvature (see Fig. 6). Then we perform a linear opening by reconstruction of size 15, then a linear closing by reconstruction of size 15, and finally a linear opening of size 29. This alternating filter removes patterns corresponding to case 3b, and in most cases patterns corresponding to case 2. These sizes were chosen for typical $512 \times 512 \times 8$ images of the retina. Values should be adjusted to the size of the vessel-like pattern. We will discuss this matter in Section VIII. Failing to adjust those parameters can lead to the removal of some apparently interesting features. The algorithm was designed to segment the main vessels and remove all possible false detection under various kinds of noise. Another strategy may simply require a different alternating filter, thus we will not deal with the adjustment of this last parameter in our discussion.

C. Evaluation of the Curvature using the Laplacian

Let C be a regular curve contained in S, passing through $p \in S$ (see Fig. 7). Let k be the curvature of C at p and $\cos \theta = n \cdot N$, where n (resp. N) is the normal vector to C (resp. S) at p. The number $k_n = k \cos \theta$ is called the normal curvature of $C \subset S$ at p, and principal curvatures are the two extrema of k_n when C varies. A detailed general method for curvature calculation can be found in [14]. The top hat filter simplifies the image before
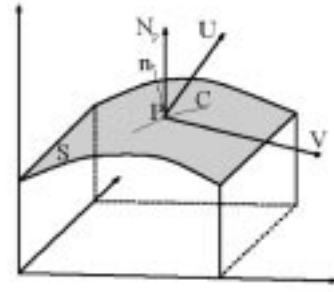

Fig. 7. Differential elements of the image.

curvature calculation in order to compute a first order estimation that is less computationally expensive than in [7].

We assume that the first filter leads to an image that locally looks like one of the three cases described in Fig. 5. Hence, for any point $p \in \mathbb{R}^2$ of image S, if k_1 and k_2 are the principal curvatures of the surface S at p then we either have $k_1 \simeq 0$ or $|k_1| \ll |k_2|$. In Fig. 5, we have denoted by U the principal direction corresponding to k_1, and V the normal direction, corresponding to k_2. We will always use these local coordinates in the following.

In order to describe these simplifications with respect to the functional S, we will express the former approximation as: $\partial S/\partial x \simeq 0$, $\partial^2 S/\partial x^2 \simeq 0$ and $\partial^2 S/\partial xy \simeq 0$. It simplifies the computation of matrices called the first and second fundamental forms that are used to compute the curvatures (see [14]).

The first fundamental form[1] in the basis (U, V) is given by

$$F_1 = \begin{bmatrix} 1 + \left(\dfrac{\partial S}{\partial x}\right)^2 & \left(\dfrac{\partial S}{\partial x}\right)\left(\dfrac{\partial S}{\partial y}\right) \\ \left(\dfrac{\partial S}{\partial x}\right)\left(\dfrac{\partial S}{\partial y}\right) & 1 + \left(\dfrac{\partial S}{\partial y}\right)^2 \end{bmatrix}.$$

It is thus simplified into

$$F_1 \simeq \begin{bmatrix} 1 & 0 \\ 0 & 1 + \left(\dfrac{\partial S}{\partial y}\right)^2 \end{bmatrix}.$$

The normal vector at point p is given by

$$N_p = \frac{\left(0, -\dfrac{\partial S}{\partial y}, 1\right)}{\sqrt{1 + \left(\dfrac{\partial S}{\partial y}\right)^2}}.$$

The second fundamental form[2] is given by

$$F_2 = \frac{1}{\sqrt{1 + \left(\dfrac{\partial S}{\partial y}\right)^2}} \begin{bmatrix} \left(\dfrac{\partial^2 S}{\partial x^2}\right) & \left(\dfrac{\partial^2 S}{\partial xy}\right) \\ \left(\dfrac{\partial^2 S}{\partial xy}\right) & \left(\dfrac{\partial^2 S}{\partial y^2}\right) \end{bmatrix}$$

[1]The natural inner product induces an inner product on the tangent plane whose matrix is the first fundamental form.

[2]If N_p is the Gaussian map and dN_p its differential form defined on the tangent plane, then F_2 is the matrix of the inner product: $v \to -dN_p(v) \cdot v$.

which we simplify into

$$F_2 \simeq \frac{1}{\sqrt{1 + \left(\frac{\partial S}{\partial y}\right)^2}} \begin{bmatrix} 0 & 0 \\ 0 & \left(\frac{\partial^2 S}{\partial y^2}\right) \end{bmatrix}.$$

As proved in [14], the principal curvatures are the eigenvalues of the Weingarten endomorphism whose matrix is

$$W = F_1^{-1} \cdot F_2 \simeq \left(1 + \left(\frac{\partial S}{\partial y}\right)^2\right)^{-3/2} \begin{bmatrix} 0 & 0 \\ 0 & \left(\frac{\partial^2 S}{\partial y^2}\right) \end{bmatrix}.$$

We deduce that $k_1 \simeq 0$, $k_2 \simeq (1 + (\partial S / \partial y)^2)^{-3/2}(\partial^2 S / \partial y^2)$. As was expected, $|k_1| \ll |k_2|$. We notice that $(\partial^2 S / \partial x^2) + (\partial^2 S / \partial y^2)$ has the same sign as k_2 (since $\partial^2 S / \partial x^2 \simeq 0$), and is independent of the frame.

Hence, the sign of the Laplacian can be used as a good approximation of the sign of the curvature. Experiments were always found to be in accordance with this approximation (see Fig. 6).

IV. MAIN ALGORITHM

We can summarize our algorithm as follows:

$$S_{op} := \gamma_{S_0}^{rec}(\text{Max}_{i=1\ldots12}\{\gamma_{L_i}(S_0)\})$$
$$S_{sum} := \sum_{i=1}^{12}(S_{op} - \gamma_{L_i}(S_0)).$$

This transformation (a sum of top hats) reduces small bright noise and improves the contrast of all linear parts. Vessels could be manually segmented with a simple threshold on S_{sum}. However, most images contain noisy data requiring further treatment, hence, the computation of the curvature

$$S_{lap} := \text{Laplacian}\left(\text{Gaussian}_{\sigma=7/4}^{\text{width}=7\,\text{px}}(S_{sum})\right).$$

Then the alternating filter, leading to the final result

$$S_1 := \gamma_{S_{lap}}^{rec}(\text{Max}_{i=1\ldots12}\{\gamma_{L_i}(S_{lap})\})$$
$$S_2 := \phi_{S_1}^{rec}(\text{Min}_{i=1\ldots12}\{\phi_{L_i}(S_1)\})$$
$$S_{res} := (\text{Max}_{i=1\ldots12}\{\gamma_{L_i}^2(S_2)\} \geq 1).$$

A PC Pentium 133 MHz with 16 MB of memory runs this algorithm on a $512 \times 512 \times 8$ image in less than 3 minutes. Note that the program was written in Visual Basic under Aphelion, an image understanding and processing software package, and that a C program would run much faster. Algorithmic improvements can also be considered (see [15]).

V. RESULTS ON DIGITAL RETINAL ANGIOGRAPHY

This algorithm has been tested on a database of about 200 angiographies, from patients with various abnormalities. The majority of the images were taken directly with a digital camera, but the database image also contains photographs digitized with a scanner. The typical image size was $512 \times 512 \times 8$, however the database included images as big as $1536 \times 1024 \times 8$. Robustness was evaluated at this stage on noisy images from the late
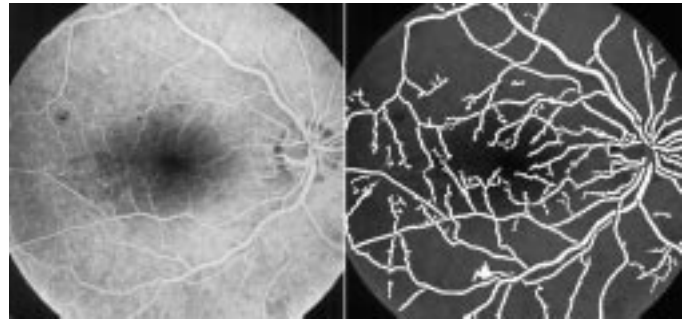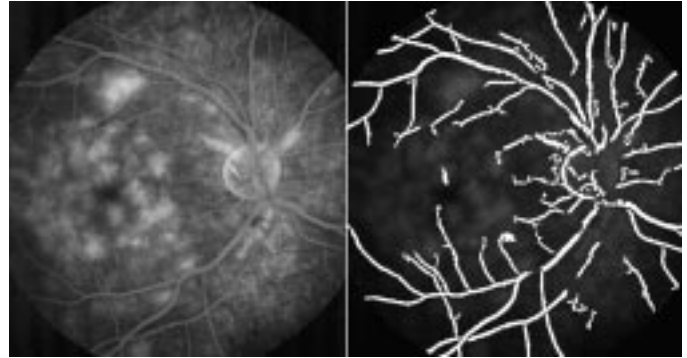

Fig. 8. Low contrast image.
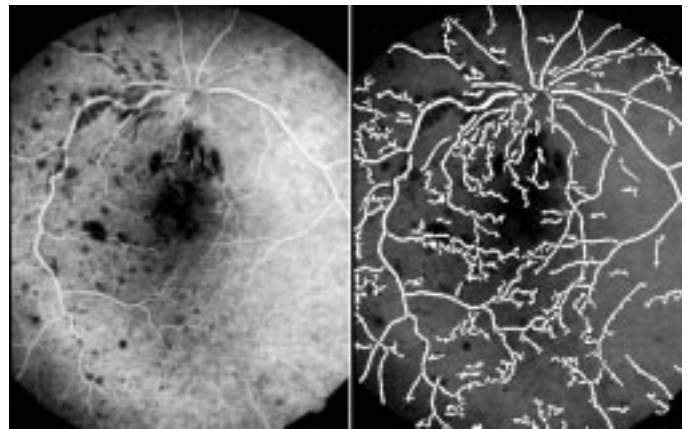

Fig. 9. Late diffusion time.

Fig. 10. Image with many dark patterns.

diffusion time (Fig. 9) and low-contrast images (Fig. 8). Images from normal eyes produce nearly perfect images (Fig. 17)

We have encountered false detection in the following cases:
- hyper-fluorescence that looks linear (Fig. 11, center bottom blob);
- black zone next to a brighter zone (Fig. 10);
- round linear bright structures are mistaken for vessels, and appear as white isolated circles.

Most of those problems are rare and related to some disease, they may be problematic when they are connected to the vascular tree (which occurred once but was not significant). Parts of vessels were not detected mostly in the late diffusion phases, and when they were hidden by some wide hyper-fluorescence (see Fig. 12, left) and in case of very low contrast (Fig. 13). In every case, the detection was in accordance with the description we gave in Section III-B: some nonvascular patterns simply fit
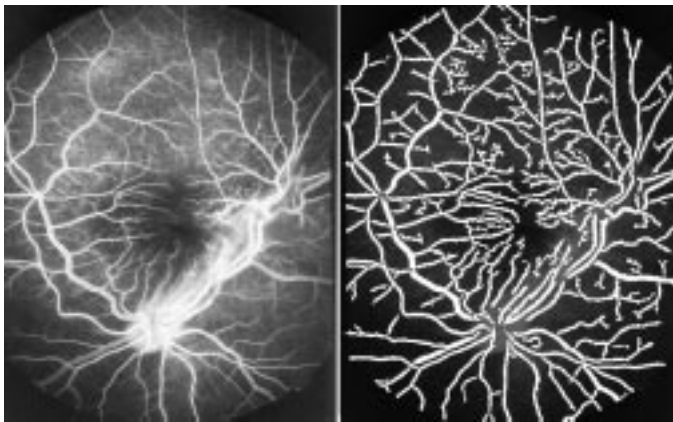
Fig. 11.   Diffusion of the dye outside the vessel.
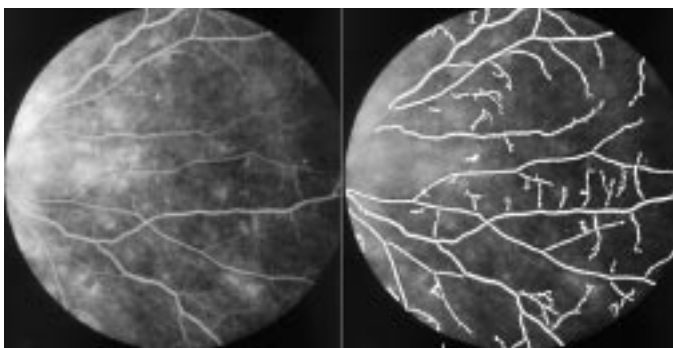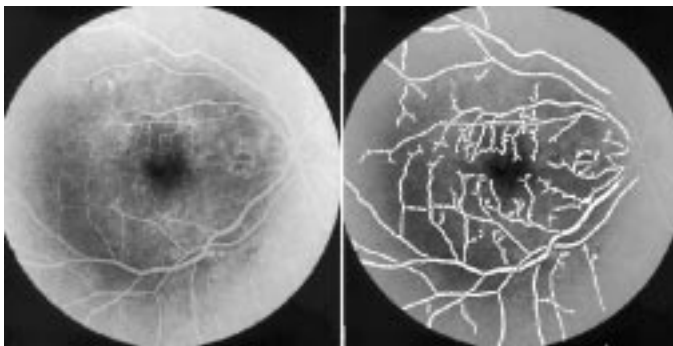

Fig. 12.   Image on a detail.

Fig. 13.   Other case, with a very low contrast.

the same model. The limit of detectable contrast is visible in Fig. 13.

Results consist of binary images superimposed upon the original image multiplied by a factor of 0.4.

VI. GENERALIZATION TO OTHER RETINAL IMAGES

The algorithm has been adapted to other types of retinal images: green images and color images of the eye fundus.

Green images of the retina are taken by physicians with green filters, and color images represent the natural colors of the eye fundus. In such images, vessels are less contrasted than in angiographic images in the state of complete diffusion (in mid-phase), and they contain less information: smaller branches of the vessel tree are simply not in the image. Each type of image is designed
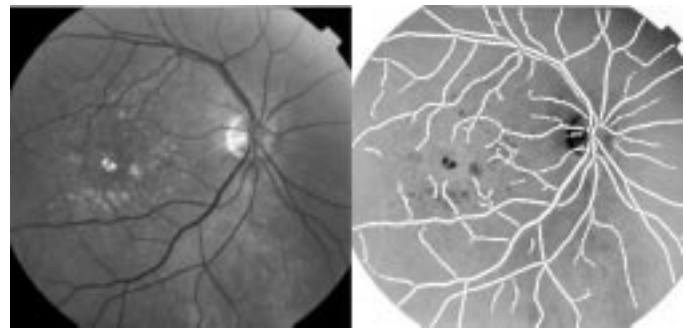
Fig. 14.   Green image from diabetic patient.[3]

to detect specific patterns. In order to bring together the information contained in all the images of a series of tests, it may be very useful to be able to register images of different types (see [13]). Since images may be very different, correlation techniques or other techniques that use the knowledge of a neighborhood may be hazardous. It seems necessary to use an invariant feature as a frame. Vessels are certainly the most appropriate pattern to use as a frame, therefore their segmentation in various types of images is of the utmost interest.

A. Green Images of the Eye Fundus

In these images, the vessels appear dark, hence the preprocessing step is a simple inversion of the gray values. It is followed by the main algorithm, no other processing is necessary. As expected, results may be less refined than with angiographic images (fewer vessels are visible), but they are still very precise and in accordance with the information contained in the image. The algorithm has been applied to several images from diabetic patients (see Fig. 14).

B. Color Images of Eye Fundus

Color images from transparent negatives developed on paper are digitized in RGB with a scanner. The blue band appears to be very weak and does not contain much information. The vessels appear in red, however the red band usually contains too much noise or is simply saturated since most of the features emit a signal in the red band. Imitating physicians we have used the green band. Inversion was performed before applying the main algorithm. The image quality was poorer than for green images of the retina, both because of a bad exposure to light and because of the development on paper. As a consequence, results appear to be less robust than in the former case, however they seem sufficient to define a frame (see Figs. 16 and 17 for a healthy eye). This algorithm has been tried on 31 images (of poor quality) from ill patients and two images of normal eyes. Fourteen images (including the two of the normal eyes) were correctly segmented with most of the vascular tree detected (see Fig. 15), but in the remaining 19 images too few vessels were detected. These results can be attributed to the lack of contrast at the end of the digitization process, which is worse in our case because of the nature of the illness. The contrast of the retina is thus lowered

---

[3]Since the green image has dark vessels, it has been inverted before superimposing vessels.

[4]Since the image has dark vessels, it has been inverted before superimposing vessels.
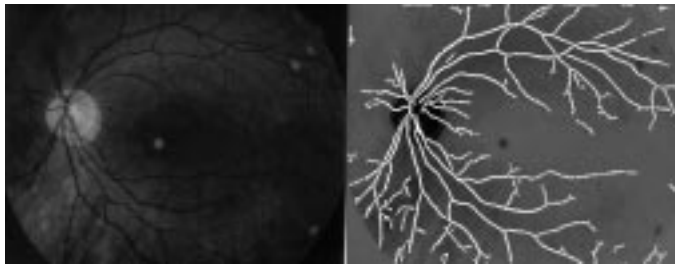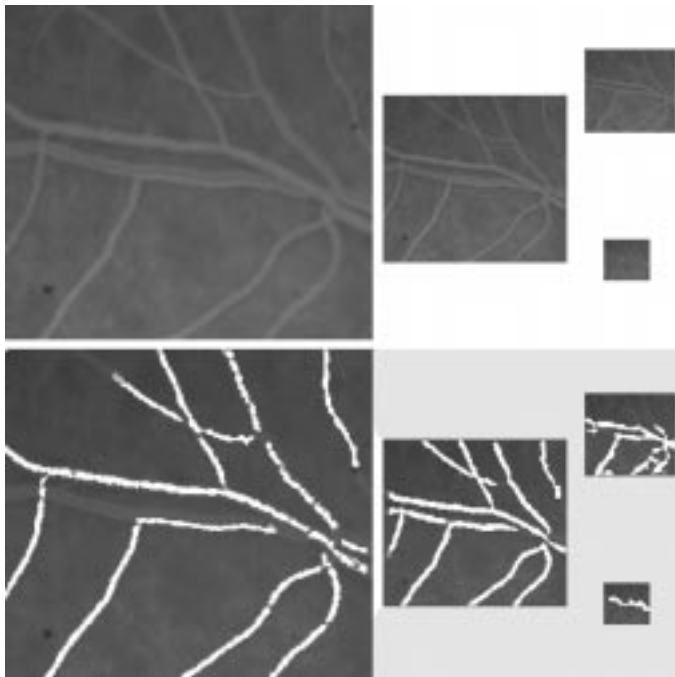
Fig. 15.   Green component of a color image.[4]

Fig. 17.   Image from an angiography of a normal eye.

Fig. 16.   Different scales of an angiographic image.

Fig. 18.   Image 17 with an addition of 100 in a selected box.
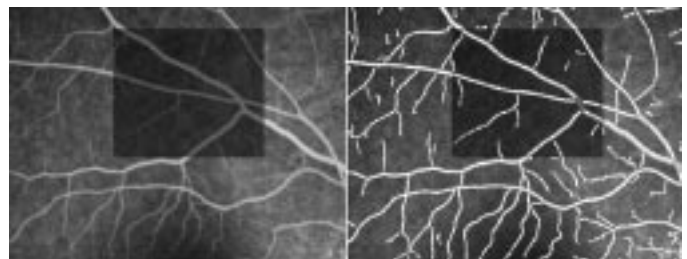
Fig. 19.   Image 17 with a division by 2 in a selected box (ROI).

by the signal coming from lower layers which are more visible. Further preprocessing for contrast enhancement, specific to the disease, has allowed a full recovery of the vascular tree in the whole set of images, however we think that a better digitization procedure should be considered in order to have a better treatment for images with low contrast in the green plane. The algorithm should also be tested on a wider range of illnesses.

VII. DISCUSSION ON THE ROBUSTNESS AND THE ACCURACY OF THE ALGORITHM

We have evaluated the performance of our algorithm on angiographic images modified by various noise additions or geometric transformations. Robustness regarding scale, noise, contrast, and accuracy will be discussed.

A. Robustness with Respect to Changes of Scale

Mathematical morphology transformations are known to be sensitive to changes of scale. Since a large part of our algorithm relies on such transformations, scale effects cannot be avoided. However, the algorithm has proved to be efficient on a wide scale of Gaussian profiles (from capillaries to big vessels). This property is due to the reconstruction procedure. Apart from the very last opening and the tophats, all openings are computed
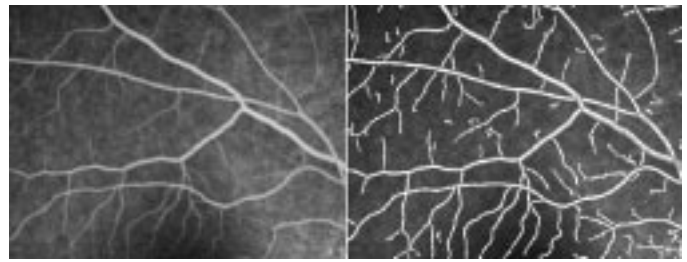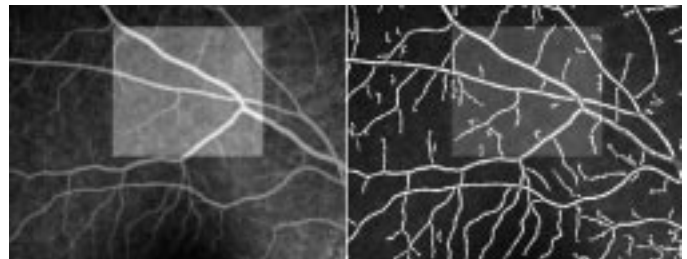
with reconstruction allowing the recovery of smaller vessels connected to the detected area. The scale effect is encountered in two parts of the algorithm: 1) during the sum of top hats, big vessels are excluded when their profiles are larger than the first structuring element and 2) during the very last opening, vessels that are not longer than the last structuring element or that appear tortuous compared to this structuring element are removed.

Fig. 16 illustrates this behavior for vessel detection.

B. Robustness with Respect to Different Types of Noise and Changes in Contrast

Various types of noise and transformation were applied to an angiographic image of the retina. Results show that the algorithm is not sensitive to sudden changes in the global gray level: addition of the value 100 that corresponds to the height of the Gaussian profile (Fig. 18), and division by a factor 2 (Fig. 19) were tested. The addition of Gaussian noise (Fig. 20) removes some capillaries but respects the global structure. The addition of uniform noise (Fig. 21) is much more destructive, although parts of the big vessels still remain. Histogram equalization (Fig. 22) creates extra noisy branches that are mistaken for capillaries.

According to the various results, the algorithm is found robust with respect to contrast change except for small areas. The addition of 100 does not change anything in the selected box, however the division by a factor of two decreases every gray
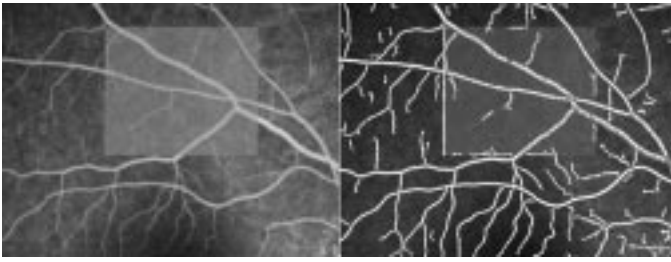
Fig. 20. Image 19 with added Gaussian noise of mean 75 and standard deviation 10 in the ROI. A vertical noisy line, two pixels wide, was also added.
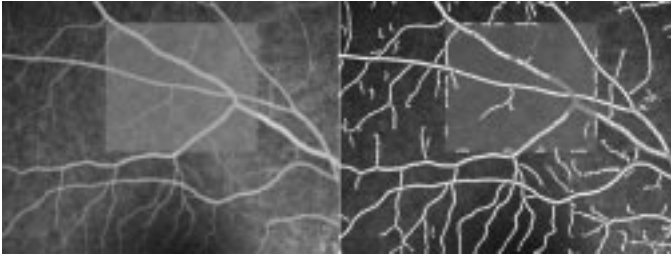

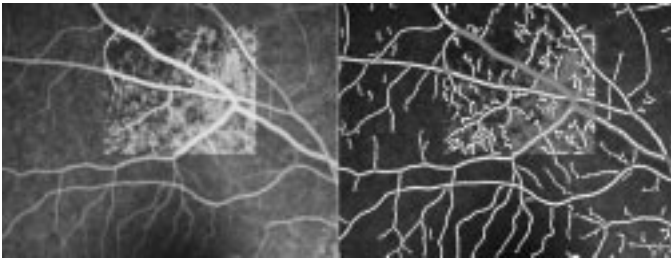Fig. 21. Image 19 with added uniform noise in the range (37,113) in the ROI.

Fig. 22. Histogram equalization in the selected box.

Fig. 23. Original image.

(a)   (b)

(c)   (d)

Fig. 24. Several edge detection algorithms: (a) morphological gradient, (b) Sobel edge detector, (c) matching filter, and (d) proposed algorithm.

level, which affects the smaller capillaries. The tophat filter is then less efficient on capillaries, even though some of them are preserved by the reconstruction. Results are less affected by Gaussian noise than by uniform noise, and histogram equalization produces worse results because it creates false detection. The reconstruction as well as the curvature evaluation are disturbed by the noise because it modifies the connectivity of the vascular structures.

C. Accuracy Evaluation

The algorithm has been designed to detect patterns with Gaussian profile limited at the inflection point. As a consequence, experiments show that small capillaries appear larger than we would think. This behavior is due to the Gaussian filter that is used before computation of the Laplacian. It was tested by drawing a straight line—two-pixels wide—inside an image of the retina, with gray value equal to the mean gray value of the surrounding vessels. The result was a set of points that contained the drawn line and included part of the line dilated by one pixel. A few pixels of the dilated line were missing because the surrounding texture had changed the location of the inflection point. This effect can be seen in Fig. 20 which contains a two pixel-wide vertical line. In proportion, small vessels will thus appear wider than their real size.
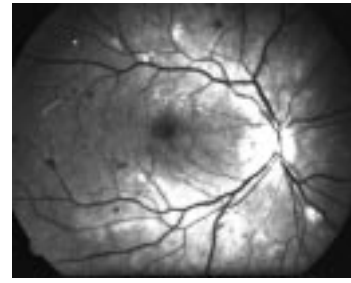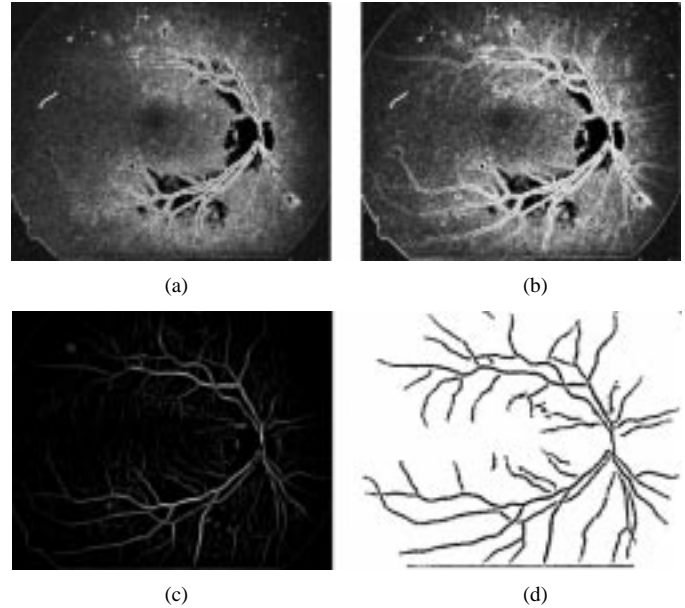
VIII. COMPARISON WITH OTHER METHODS: DISCUSSION

An original image is given in Fig. 23, and we apply several filters to this image, including the algorithm that we propose. We then discuss the quality of the result with regard to the ability to use this segmentation for registration. For this purpose, we define four criteria:

1) good qualitative detection of the biggest vessels;
2) small proportion of false detection;
3) significant number of bifurcation points can be visually identified in the vascular structure;
4) segmented structure is connected.

These criteria are qualitative and will thus require a short discussion.

We have applied some edge detectors (Sobel, morphological edge detector), the matching filter [11] based on the Canny edge detector, as well as the algorithm that we propose to the image 23. As was foreseeable, the Sobel and the morphological edge detector [Fig. 24(a) and (b)] produce parallel edges, the biggest vessels are easily recognizable whereas smaller vessels appear less contrasted. They satisfy criterion 3) however, an algorithm for the detection of parallel edges is necessary to achieve the other criteria. The accuracy of bifurcation points will depend on the quality of the post-treatment as well as the proportion of

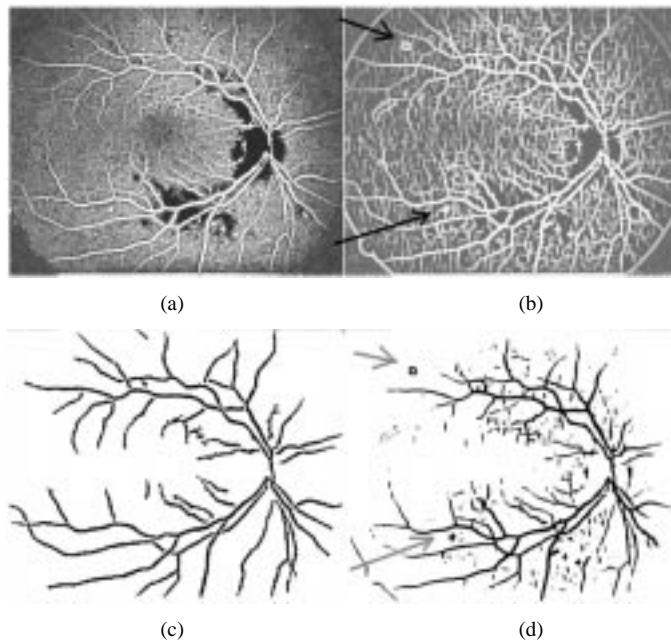[5]Image generously provided by Dr. C. Heipke, reproduced from [16].

Fig. 25. $\begin{smallmatrix} a & c \\ b & d \end{smallmatrix}$: (a) sum of tophats with histogram equalization, (b) automatic threshold from the proposed algorithm, (c) the matching filter with histogram equalization, and (d) manual threshold on (c).
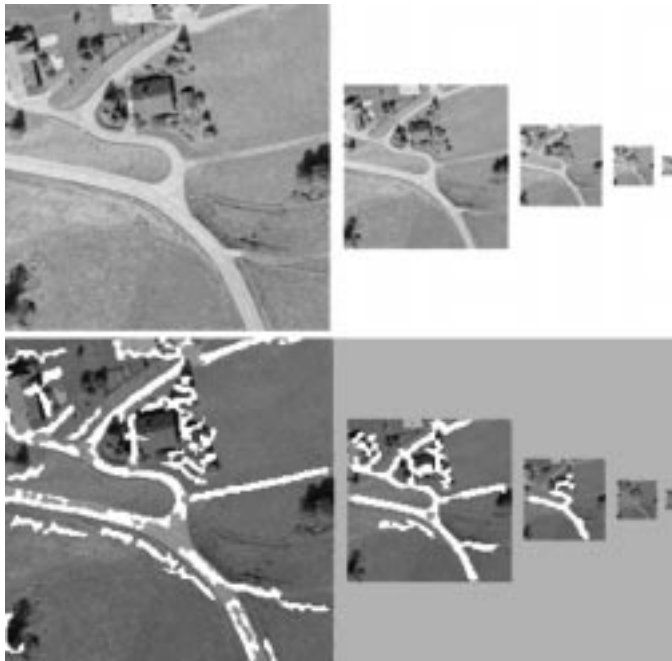

Fig. 26.   Different scales of an outdoor image with a road.[5]

false detection, however it is likely that criterion 2) will not be satisfied since nonvascular structures are also detected as edges.

The matching filter algorithm Fig. 24(c) produces an image of good quality, satisfying criteria 1) and 3) for the biggest vessels, however some smaller vessels of poor contrast are only partially detected. The connectivity of the structure (criterion 4) is not guaranteed along the same capillary, as can be seen when we threshold the image [see Fig. 25(d)]. Since this algorithm also results in some false detection (see the two arrows in Fig. 25) and does not produce a clean binary image, it may be difficult to separate the good structures from the false detection.

Our method produces a binary image that is more selective. Therefore criterion 1) is not fully satisfied if we include some small vessels. However, it is the only algorithm, compared to the other three methods, achieving a very small proportion of false detection [criterion 2)], even if we use a high threshold on one of the images produced by the other three algorithms. The criteria 3) and 4) are satisfied with approximately the same quality as with the matching filter, however the algorithm that we propose will lead to less bifurcation points and less false detection. Concerning criterion 4), the algorithm that we propose creates connected linear structures that are clean but not always connected to each other. The detection of bifurcation points is thus easy.

In order to illustrate the difference between the matching filter and the algorithm that we propose, we have improved the contrast of an intermediate image [Fig. 25(a) and (c)]. These figures are very similar with respect to the biggest vessels, however the real difference between those methods lies in the structure of the background noise. With the matching filter the background of the image is transformed, the linear structures are more contrasted even when they are not relevant (for example when they are not connected to a big vessel). Whereas with our algorithm the background structure is noisy and does not present the same structure as the vessels. It is thus possible to eliminate the noise completely, for example using a curvature differentiation.

IX. CONCLUSIONS

An efficient algorithm for vessel-like pattern detection has been presented. Robustness and accuracy have been evaluated on different images, demonstrating that it may be useful in a wide range of retinal images. Based on a brief comparison with some other edge detection algorithms, we can conclude that the complementarity of mathematical morphology and linear transforms allows a more complete treatment. It was possible to select vessels using shape properties, connectivity, as well as differential properties like curvature. The robustness and weaknesses of the algorithm have been evaluated and explained in order to facilitate its use for the analysis of retinal images. This segmentation has been used for image registration of images of the retina [13], and it is the first step toward an automatic diagnosis software.

Even though the scope of this article is limited to eye fundus images, The reader should note that the proposed algorithm has been tested successfully on other images. In Fig. 26, the road can be described as being a tree-like edge with a Gaussian-like profile. Since this description fits our model, it is not surprising to see that the road is segmented with our algorithm. Some developments in other areas cannot be excluded.

REFERENCES

[1] H.-C. Liu and M. D. Srinath, "Partial shape classification using contour matching in distance transformation," *IEEE Trans. Pattern Anal. Machine Intell.*, vol. 12, pp. 1072–1079, Nov. 1990.

[2] D. Marr and E. Hildreth, "Theory of edge detection," *Proc. R. Soc. Lond.*, vol. 207, pp. 187–217, 1980.

[3] N. K. Ratha, K. Karu, S. Chen, and A. K. Jain, "A real-time matching system for large fingerprint databases," *IEEE Trans. Pattern Anal. Machine Intell.*, vol. 18, pp. 799–812, Aug. 1996.

[4] L. G. Brown, "A survey of image registration techniques," *ACM Comput. Surv.*, vol. 24, no. 4, pp. 352–376, 1992.

[5] W. Hoff and N. Ahuja, "Surface from stereo: Integrating feature matching, disparity estimation, and contour detection," *IEEE Trans. Pattern Anal. Machine Intell.*, vol. 11, pp. 121–136, Feb. 1989.

[6] R. Lengagne, P. Fua, and O. Monga, "Using crest lines to guide surface reconstruction from stereo," in *Proc. Conf. Pattern Recognition*, Aug. 1996.

[7] O. Monga, N. Armande, and P. Montesinos, "Thin nets and crest lines: Application to satellite data and medical images," INRIA, Res. Rep. 2480, Feb. 1995.

[8] J. Canny, "A computational approach to edge detection," *IEEE Trans. Pattern Anal. Machine Intell.*, vol. 8, pp. 679–698, June 1986.

[9] F. Zana and J. C. Klein, "Robust segmentation of vessels from retinal angiography," in *Int. Conf. Digital Signal Processing*, Santorini, Greece, July 1997, pp. 1087–1091.

[10] J. Serra, *Image Analysis and Mathematical Morphology*. London, U.K.: Academic, 1982.

[11] S. Chaudhuri, S. Chatterjee, N. Katz, M. Nelson, and M. Goldbaum, "Detection of blood vessels in retinal images using two-dimensional matched filters," *IEEE Trans. Med. Imag.*, vol. 8, no. 3, pp. 263–269, 1989.

[12] R. Nekovei and Y. Sun, "Back-propagation network and its configuration for blood vessel detection in angiograms," *IEEE Trans. Nueral Networks*, vol. 6, pp. 64–72, Jan. 1995.

[13] F. Zana and J. C. Klein, "A registration algorithm of eye fundus images using vessels detection and hough transform," *IEEE Trans. Med. Imag.*, submitted for publication.

[14] M. P. Do Carmo, *Differential Geometry of Curves and Surfaces*. Englewood Cliffs, NJ: Prentice-Hall, 1976.

[15] F. Cheng and A. N. Venetsanopoulos, "An adaptive morphological filter for image processing," *IEEE Trans. Image Processing*, vol. 1, pp. 533–539, Apr. 1992.

[16] C. Heipke, "Overview of image matching techniques," Munchen University, http://dgrwww.epfl.ch/phot/publicat/wks96, April 1996.

[17] M. J. Cree, J. A. Olson, K. C. McHardy, J. V. Forrester, and P. F. Sharp, "Automated microaneurysm detection," in *Int. Conf. Image Processing*, 1996.

[18] T. R. Friberg, J. Lace, J. Rosenstock, and P. Raskin, "Retinal microaneurysm count in diabetic retinopathy: Color photography versus fluorescein angiography," *Can. J. Ophthalmology*, vol. 22, no. 4, pp. 226–229, 1987.

[19] B. Lay, *Analyze Automatique des Images Angiofluorographiques au Cours de la Rétinopathie Diabétique*: Ecole Nationale Supérieure des Mines de Paris, 1983.

[20] P. K. Sahoo, S. Soltani, A. K. C. Wong, and Y. C. Chen, "A survey of thresholding techniques," *Comput. Vis., Graph., Image Process.*, vol. 41, pp. 233–260, 1988.

Frédéric Zana graduated in theoretical mathematics from the Ecole Normale Supéerieure de Paris (ENSP), Paris, France, in 1993, received the M.S. degree in computer science from the ENSP in 1994, and the M.S. degree in macroeconomics from ENSP in 1996. Since 1996 he has been pursuing the Ph.D. degree student at the Centre de Morphologie Mathématique, Ecole des Mines de Paris.

Jean-Claude Klein received the Ph.D. degree in electronics from the University of Nancy, France, in 1975.

Since 1969, he has been with the Centre de Morphologie Mathématique, Ecole des Mines de Paris, Paris, France, where he has been in charge of the research group devoted to the design of dedicated hardware architectures applied to real-time image processing and the design of a continuous blood glucose monitoring system.